Macromolecules

pubs.acs.org/Macromolecules
Article

Stability Descriptors for (Benz)imidazolium-Based Anion Exchange Membranes

Fabian P. Tipp, Kate Fraser, Mohammad J. Eslamibidgoli, Kourosh Malek, Steven Holdcroft, and Michael H. Eikerling*

Cite This: Macromolecules 2024, 57, 1734–1743

ABSTRACT: (Benz)imidazolium-based polymers are a promising class of anion exchange membrane materials for alkaline fuel cells and electrolyzers. This study focuses on the alkaline stability of (benz)imidazolium-based compounds by exploring the relationship between molecular structure and degradation rate. A correlation analysis, using ab initio quantum chemical calculations, reveals suitable stability descriptors for three types of compounds, namely, benzimidazoliums, penta-substituted imidazoliums, and bis-arylimidazoliums. The strongest correlation is found between the Gibbs free energy change of the C-2 hydroxide attack step and the experimental stability. Notably, the activation energy and Gibbs free energy change of the hydroxide attack on C-2 display a high correlation. Identifying computationally efficient descriptors is a crucial prerequisite for the screening and inverse molecular design of imidazolium-based compounds with high alkaline stability.

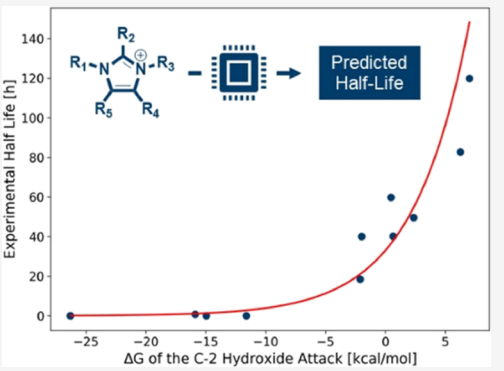

INTRODUCTION

Sustainable and environmentally friendly energy technologies will be crucial in supplying the global energy demand and slowing climate change. Green hydrogen is set to play an important role in the future energy ecosystem.[1−3] However, successful implementation of green hydrogen as an energy carrier requires hydrogen to be produced using water electrolyzers (WEs), powered by excess renewable energy (e.g., solar or wind). This hydrogen can then be stored and used on demand in fuel cells (FCs) to generate electrical energy.

WEs and FCs can operate in acidic or alkaline environments. While acidic WEs achieve high power densities, platinum group metal (PGM) catalysts that do not corrode in low pH are required.[4] Utilization of significant amounts of PGMs increases costs and poses a significant supply risk.[5] Conversely, alkaline WEs and FCs eliminate the need for PGMs.[6] Yet, finding an organic ion-conducting medium with sufficient hydroxide ion conductivity and stability remains an open area of research.[7,8]

Anion exchange membranes (AEMs) are solid polymer electrolytes composed of positively charged groups that are bound to a polymer matrix. For successful integration into devices, AEMs must be synthesized to exhibit sufficient chemical and mechanical stability along with high anion conductivity. Incorporating these properties into AEMs remains a critical challenge to be addressed.[9−12]

Quaternary ammonium (QA) ions are most commonly used as cations in AEMs, given the comparatively simple synthesis[13] along with good mechanical stability;[14] however, their low chemical stability has hindered further development.[15] Various other organic cations have emerged as a basis for AEMs including tetraalkylammoniums,[16,17] phosphoniums,[18,19] piperidiniums,[20] and guanidiniums.[21] Notably, imidazoliums, bis-arylimidazoliums, and benzimidazoliums have drawn considerable attention due to their high hydroxide conductivity and stability (Figure 1).[7,22−30]

Delocalization of the positive charge over the (benz)imidazolium ring renders the cation less susceptible to hydroxide attack.[31] However, attaining adequate alkaline stability for integration into alkaline electrochemical devices

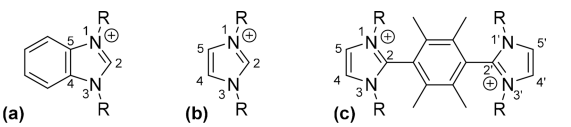

Figure 1. Compounds studied in this work are based on three distinct backbones: (a) benzimidazolium, (b) imidazolium, and (c) bis-arylimidazolium, with the numbering scheme provided for the most significant atoms.

Received: November 9, 2023
Revised: January 8, 2024
Accepted: January 17, 2024
Published: February 6, 2024

remains challenging due to the two irreversible hydroxide-mediated degradation pathways that are shown in Figure 2: (a) dealkylation of the N-1/N-3 substituent via a S_N2 type reaction and (b) a nucleophilic addition−elimination at C-2.[32−36]

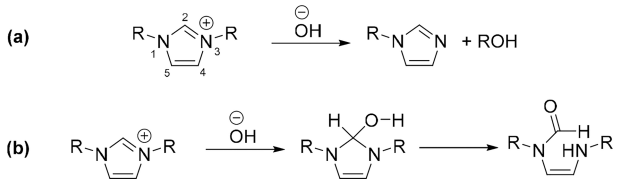

Figure 2. Two irreversible degradation pathways of imidazolium-based compounds, a dealkylation of the N-1/N-3 substituent (a) and a ring-opening nucleophilic addition−elimination at C-2 (b).[32]

The alkaline stability of (benz)imidazolium-based compounds is significantly influenced by their chemical structure.[22,31,37] However, directly comparing stability measurements for various reported compounds across the experimental literature is challenging for several reasons. Firstly, various experimental techniques were used for monitoring the degradation state such as measurement of ion exchange capacity, ^{1}H NMR spectroscopy, or conductivity measurements.[12] Secondly, chemical conditions vary widely in terms of hydroxide concentration, solvents, degree of hydroxide hydration, temperature, and the specifics of solvent-less degradation tests through dynamic vapor sorption.[12,38] Due to the variability of test conditions, comparison of different compounds can be cumbersome to perform and misleading, and the high resource and time demand of experimental stability tests render retesting of compounds under different conditions impractical. Quantum chemical simulations can circumvent this problem, as they are orders of magnitude cheaper and faster to perform, compared to physical experiments. However, a computational descriptor of a compound's alkaline stability is required for an effective quantum chemical assessment of AEM candidate materials.

Identifying stability descriptors of imidazolium-based compounds with ab initio quantum chemical calculations will enable highly efficient computational screening of such compounds and thus furnish the path towards inverse molecular design. Even when only considering a penta-substituted imidazolium with a set of 20 possible substituents, millions of different structures are possible; preselecting based on computationally predicted stability can greatly reduce the search space of AEM materials.

An approach to assess alkaline stability with ab initio quantum mechanical simulations involves calculation of the hydroxide-induced degradation reaction energetics. Through these studies, it has been determined that the nucleophilic addition−elimination at C-2 is the main degradation pathway, and that the choice of substituents impacts the energy barriers associated with this pathway.[32,39] Further systematic efforts are needed to unravel correlations between the theoretical energetics of relevant degradation pathways and experimental stability data. Prior investigations have focused on the LUMO energy of compounds, where a qualitative relationship between higher LUMO energy and higher alkaline stability has been reported.[35,40] Additionally, the LUMO isosurface has been utilized, with a higher LUMO localization at the imidazolium ring promoting a hydroxide attack and therefore faster degradation.[41]

Different strategies to influence the stability of imidazolium-based compounds through adjustments to the molecular structure are reported in the literature.[31,34,40,42,43] Increasing the steric hindrance around electrophilic sites on imidazolium has been shown to be a viable approach for limiting hydroxide attacks. This can be achieved not only through substitution at the C-2 position but also through substitution at the surrounding N-1 and N-3 sites.[23,26,35,43] It has been reported that a higher LUMO energy decreases the degradation rate as

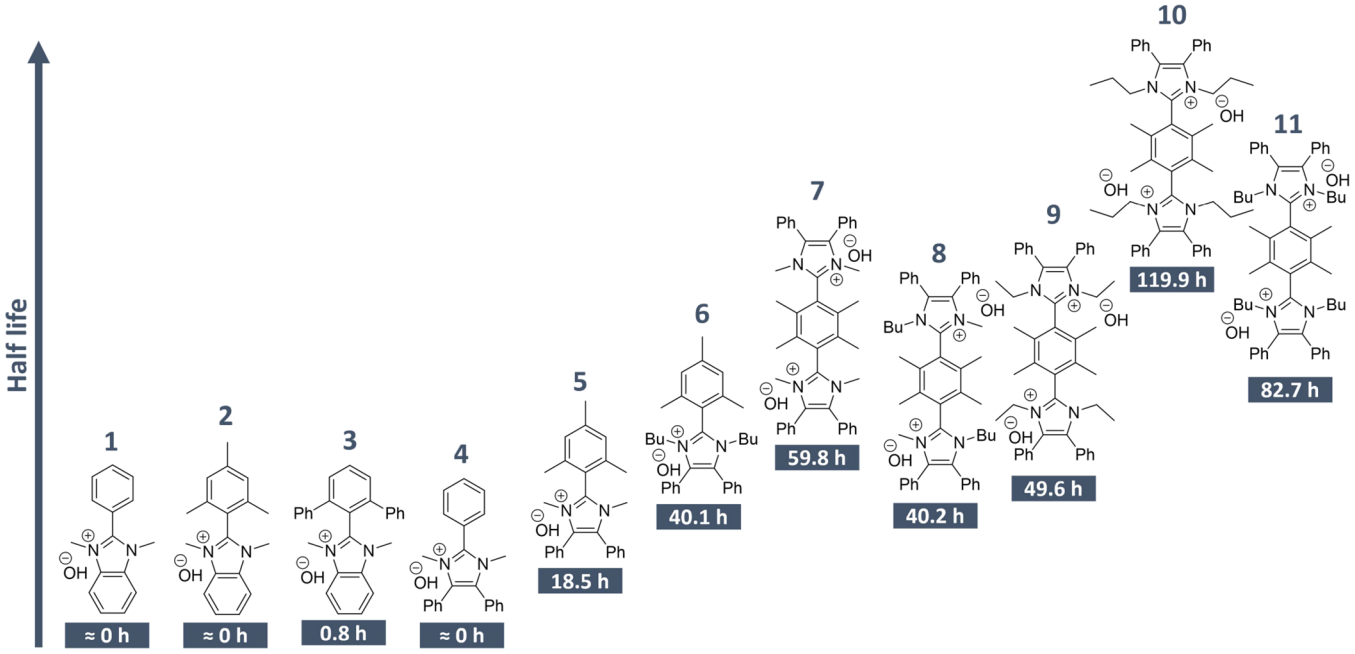

Figure 3. Compounds investigated in this study along with their half-lives in an ultradry KOH solution of DMSO/crown ether at room temperature, as reported by Fan et al.[22]

https://doi.org/10.1021/acs.macromol.3c02294
Macromolecules 2024, 57, 1734−1743

Table 1. Gibbs Free Energy Values of the Dealkylation (a in Figure 2) and the Nucleophilic Addition−Elimination Reaction (b in Figure 2) of the Studied Compound along with the Experimental Half-Lives in an Ultradry KOH Solution of DMSO/Crown Ether at Room Temperature[22a]

molecule	ΔG(a) (kcal/mol)	$\Delta G^{\ddagger}$(a) (kcal/mol)	ΔG(b first step) (kcal/mol)	$\Delta G^{\ddagger}$(b first step) (kcal/mol)	ΔG(b) (kcal/mol)	experimental half-life (h)[22]
1	−33.38	25.01	**−26.30**	**1.34**	**-31.93**	**0**
2	−31.58	25.20	−14.96	9.72	−30.53	**0**
3	−32.39	25.65	−15.89	15.04	−29.12	0.8
4	−30.96	26.62	−11.62	5.56	−22.24	**0**
5	−29.12	27.51	−2.10	15.28	−19.46	18.5
6	**−33.86**	**23.61**	−1.98	12.74	−21.45	40.1
7	−29.16	29.08	0.47	16.09	−20.17	59.8
8	−30.53	24.12	0.65	15.80	−22.11	40.2
9	−32.09	28.56	2.36	18.00	−20.52	49.6
10	**−28.47**	**30.42**	**7.02**	**20.44**	−15.08	**119.9**
11	−29.15	29.77	6.26	19.02	**−14.88**	82.7

[a]The highest and lowest energies for each reaction step are in bold. The corresponding molecular structure is depicted in Figure 3.

it hinders the nucleophilic hydroxide attack.[40] Substituting with electron-donating groups can achieve a high LUMO level.[35]

Stabilization of the cationic charge has also been exploited to inhibit degradation, as it decreases the electrophilicity of the compound and increases the LUMO energy.[40] This stabilization is achievable through appropriate substitutions at the imidazolium ring, such as with methyl groups, which stabilize the charge through $\sigma-\pi$ hyperconjugation.[34,40]

Altough several individual factors have been identified for predicting alkaline stability of these compounds, they are not yet reliable enough for large-scale scanning of novel AEM molecular compounds, and a need remains for precise and cost-effective computational descriptors that are thoroughly validated against experimental stability measurements. Identifying such descriptors has not yet been addressed, most likely due to the difficulty in collecting sufficient data for families of materials to measure their stability under alkaline conditions.

This work identifies suitable alkaline stability descriptors for imidazolium model compounds to improve the screening process of potential AEM materials. Identifying specific stability descriptors will enable high-throughput screening and the inverse molecular design of imidazolium-based materials. We utilized the experimental results by Fan et al.,[22] which tested the alkaline stability of 11 imidazolium-based compounds, as shown in Figure 3. Experimental values for the compounds' half-life were measured in an ultradry solution of 0.5 M KOH in DMSO/crown ether with a hydroxide hydration level λ = 1 at room temperature.

METHODOLOGY

Ab initio quantum chemical calculations were performed using the ORCA 5.0.3 quantum chemistry package[44] with the 6-311G(d,p)[45,46] basis set. DFT-level calculations were done with the B3LYP[47,48] functional. All DFT calculations employed a simulated water solvation environment using the conductor-like polarizable continuum model[49] with the standard parameters for water. For each compound, the following procedure was excecuted. The SMILES representation of the (benz)imidazolium cation without counterion was converted into a 3D structure using version 2022.9.4 of RDKIT.[50] To ensure that the calculations are performed with a reasonable conformer structure, a conformer scan was performed using version 2.12 of CREST[51,52] using the "--quick" parameter preset, and the lowest energy conformer was selected for further use. The conformer scan was conducted in an implicit water solvation environment using the analytical linearized Poisson−Boltzmann (ALPB) model. A hydroxide ion was placed close to the (benz)imidazolium cation, and a geometry optimization at the DFT level was performed. The hydroxide was initially positioned roughly 5 ånstroms above the plane of the imidazolium ring. The resulting structure was used as the reference structure for all calculated energetics. Starting from the reference structure, the products and intermediates of the degradation pathways were manually created, and a DFT-level geometry optimization was performed. The geometry-optimized degradation product/intermediate and reference structure were used to identify the transition state of the corresponding reaction step using the nudged elastic band method[53] at the DFT level. For each obtained structure, a frequency analysis was carried out, and it was ensured that all transition states possess only a single imaginary frequency along the reaction coordinate and that all other structures do not possess any imaginary frequencies. The Gibbs free energy of each structure is then computed based on the frequency analysis. A single-point DLPNO−CCSD(T)[54] calculation was done for each optimized structure, and the obtained electronic energy was used to replace that obtained by DFT in the contributions to the Gibbs free energy.

RESULTS

Energetics. Table 1 shows calculated values of the Gibbs free energy change for the 11 studied compounds along the two competing irreversible hydroxide attack pathways, as shown in Figure 2. The first mechanism is S_N2 dealkylation via hydroxide attack of the N1/N3 substituent (a in Figure 2). The second mechanism is the ring-opening pathway (b in Figure 2), which involves an initial attack of the hydroxide at the C-2 position (first step of b in Figure 2) followed by an opening of the (benz)imidazolium ring (second step of b in Figure 2). The corresponding experimental half-lives in an ultradry KOH solution of DMSO/crown ether at room temperature are also provided in Table 1, as reported by Fan et al.[22]

Calculated activation energies for hydroxide attack on C-2 (first step of b in Figure 2) range from 1.34 to 20.44 kcal/mol, revealing that this pathway is strongly influenced by the molecular structure of the compound. In contrast, the

https://doi.org/10.1021/acs.macromol.3c02294
Macromolecules 2024, 57, 1734−1743

activation energies of dealkylation (a in Figure 2), which span from 23.61 to 30.42 kcal/mol, indicate that the molecular structure has a limited impact on the activation barrier across all studied molecules. The higher activation barrier for dealkylation implies that this process is not the dominant degradation pathway for the studied compounds. The lower activation barrier for the C-2 hydroxide attack singles out this pathway as the dominant degradation mechanism under the studied conditions.

Plotting $\Delta G^{\ddagger}$ vs ΔG of the C-2 hydroxide attack in Figure 4a indicates a Bell–Evans–Polanyi type correlation.[55,56] While

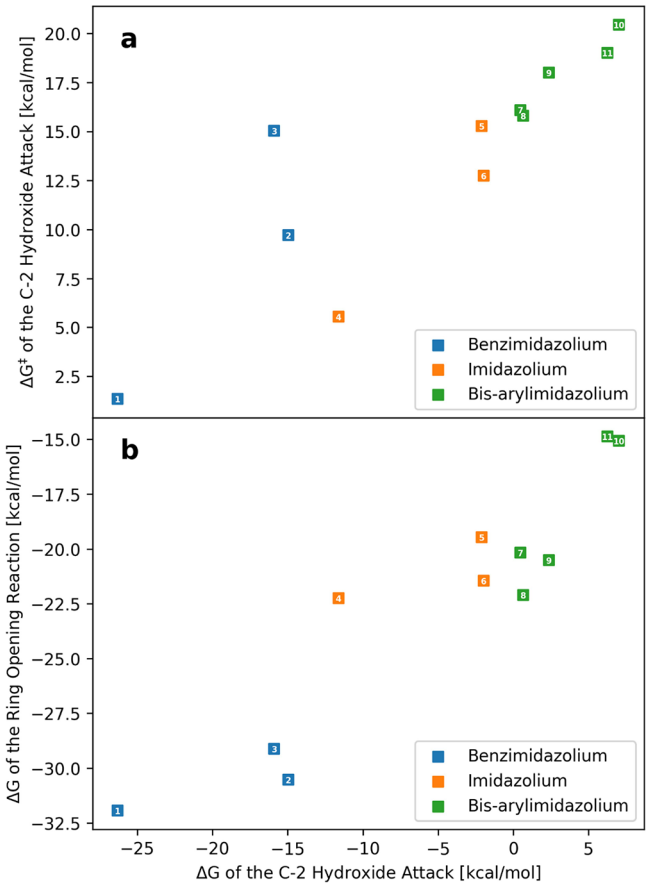

Figure 4. Scatter plot of ΔG of the C-2 hydroxide attack against $\Delta G^{\ddagger}$ of the C-2 hydroxide attack (a) and ΔG of the full ring-opening degradation pathway (b). The number in each marker of the plot corresponds to the molecule number it represents.

primarily the activation energy $\Delta G^{\ddagger}$ of the dominant degradation pathway determines the degradation rate, using this correlation, ΔG can also be used instead. The advantage is that ΔG is much less expensive to compute in comparison to $\Delta G^{\ddagger}$, especially when calculations are ought to be automatized for a high-throughput scan of materials. Additionally, ΔG of the C-2 hydroxide attack appears to be correlated with ΔG of the full ring-opening degradation pathway, as depicted in Figure 4b. A favorable C-2 hydroxide attack therefore predicts a thermodynamically stable degradation product.

Figure 5 shows the Gibbs free energy profile of the studied degradation pathways for three selected molecules 1, 5, and 10, from each class. The lower activation barrier for the C-2 hydroxide attack in comparison to the dealkylation can be observed, along with the greater range of $\Delta G^{\ddagger}$ values of the former compared to $\Delta G^{\ddagger}$ values of the later. The free energy diagrams for all compounds are included in the Supporting Information (Figures S1–S3).

To verify the predictive ability of ΔG of the C-2 hydroxide attack for the experimental half-lives, the two values are plotted against each other in Figure 6a. The natural logarithm of the experimental half-life was calculated and correlated against ΔG of the C-2 hydroxide attack to obtain a linear correlation with a coefficient of determination R^2 of 0.943 (Figure 6b). For the energetics of the dealkylation pathway, a significant correlation with the alkaline stability could not be observed. The coefficient of determination between the natural logarithm of the experimental half-lifes and ΔG (a in Figure 2) is 0.195. The scatter plot is reported in the Supporting Information (Figure S4).

Electronic Properties. While obtaining ΔG of a given reaction is computationally less expensive than calculating the corresponding $\Delta G^{\ddagger}$, it may still be too costly to compute for more than a few hundred compounds. The calculation of electronic properties such as orbital energies or distributions could be much more efficient, making a stability descriptor constructed from them very valuable for searching a sizable part of the vast chemical space of possible imidazolium-based AEM materials. One stability descriptor based on electronic properties of the imidazolium compounds proposed in the literature is the LUMO energy, with a higher LUMO energy corresponding to more stable compounds.[34,35,40,57] The correlation between LUMO energy and experimental stability of a given compound could not be reproduced for the imidazoliums investigated in this work as can be seen in Figure S5 in the Supporting Information.

It has been reported previously that the LUMO energy may not be sufficient as a lone indicator of alkaline stability and a more in-depth analysis of the LUMO must be performed. One additional aspect to consider is the LUMO isosurface, with a LUMO distribution localized on the imidazolium ring leading to lower stability by promoting a hydroxide attack.[41] For a computational stability descriptor that can be automatically generated for a given compound, analyzing a LUMO isosurface is impractical because the generated images generally require manual interpretation or advanced techniques such as machine learning. For this reason, we propose quantitatively assessing the LUMO distribution through frontier molecular orbital population analysis (FMOPA), which computes the fraction of LUMO that is localized on each atom of a given molecule. As hydroxide attacks the C-2 position, the fraction of LUMO that is localized on C-2 may be an indicator of the degree to which the LUMO distribution promotes the ring-opening degradation pathway, at least for cases in which the LUMO energy is not high enough to strongly inhibit the reaction.

In Table 2, the LUMO distribution, LUMO fraction on C-2, and the LUMO energy are reported for three selected compounds, and the full table with all studied compounds is given in the Supporting Information (Table S3). For the benzimidazolium (molecule **1**, exp. half-life ≈0 h), the LUMO is distributed along the C-2 substituent and the benzimidazolium ring. However, over 25% of the LUMO is localized on the C-2 atom, and the LUMO energy is the lowest of the three compounds, leading to a fast degradation by enabling a hydroxide attack. The LUMO of the more stable imidazolium (molecule **6**, exp half-life 40.1 h) is localized to roughly the same degree on the C-2 atom as it is for molecule **1**. However, the LUMO energy is significantly higher than that of molecule

https://doi.org/10.1021/acs.macromol.3c02294
Macromolecules 2024, 57, 1734–1743

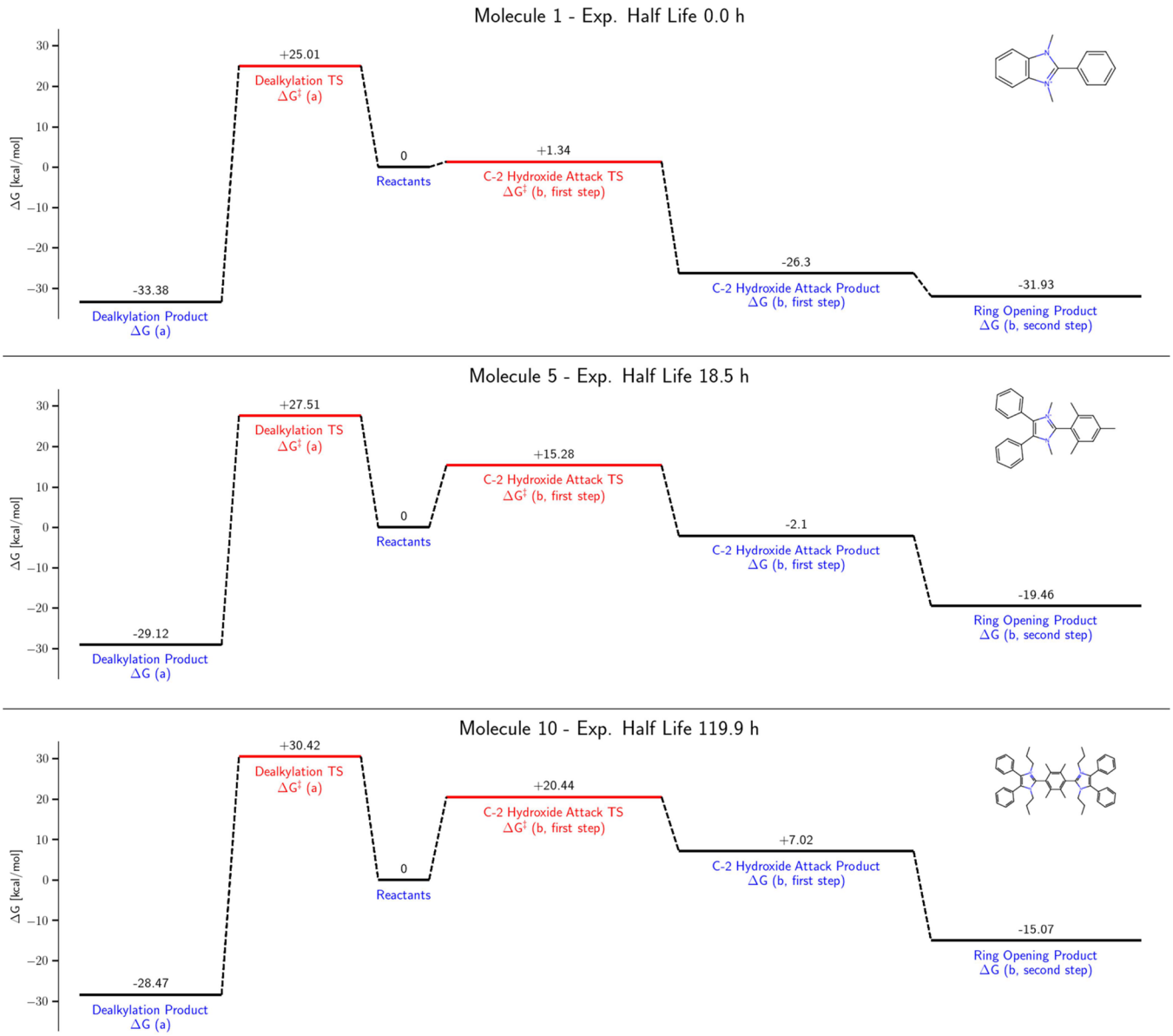

Figure 5. Gibbs free energy profile of the dealkylation (a in Figure 2) and the nucleophilic addition−elimination reaction (b in Figure 2) of three selected studied compounds.

1, inhibiting hydroxide attack. The most stable of the studied compounds is a bis-arylimidazolium (molecule **10**, half-life 119.9 h), which possesses a lower LUMO energy than molecule **6** does. However, only 8% of the LUMO is localized on each C-2 atom, which may strongly inhibit the C-2 hydroxide attack.

The product of LUMO energy and LUMO fraction localized on C-2 can be calculated to combine both values into one stability descriptor. This descriptor correlates moderately well with ΔG of the C-2 hydroxide attack, as depicted in Figure 7. The moderate correlation with an R^2 of 0.733 is expected, as only electronic and no steric effects are included. However, the descriptor is computationally very efficient and may aid in a coarse scan of potential compounds; e.g., the relative stabilities of benzimidazolium, imidazolium, and bis-arylimidazolium were correctly predicted.

DISCUSSION

The identified electronic and energetic descriptors enable a high-throughput scan to find imidazolium-based compounds with high alkaline stability. This is our current work in progress and will be published in the near future. Additionally, the descriptors support the understanding of the intricate relationship between the chemical structure and alkaline stability. One aspect of interest is whether differences in alkaline stability between different compounds stem from electronic or steric effects. For the studied systems, it is difficult to separate the two effects, as both are intertwined. An illustrative example is the difference between studied molecules **1** and **2**, which were chosen as they present the smallest compounds and as they differ only in their C-2 substituent with the prior possessing a phenyl group and the later a mesityl group. This difference in C-2 substituent leads to molecule **2** having an ΔG of the C-2 hydroxide attack that is about 11 kcal higher than that of molecule 1. While the absolute values are so low (−26.30 and

https://doi.org/10.1021/acs.macromol.3c02294
Macromolecules 2024, 57, 1734−1743

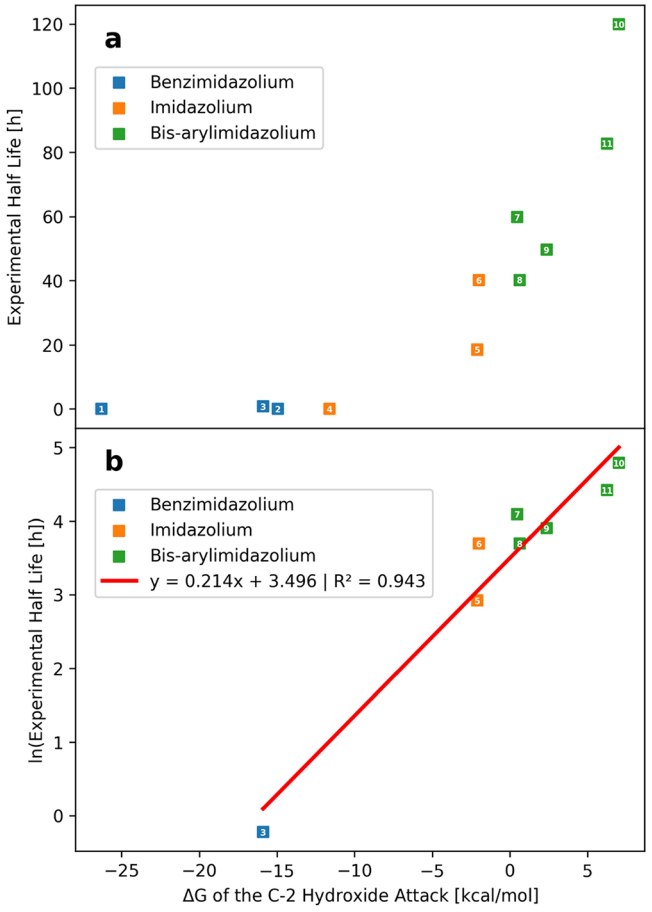

Figure 6. Scatter plot of ΔG of the C-2 hydroxide attack and the experimental half-life (a: unmodified; b: its natural logarithm) in an ultradry KOH solution of DMSO/crown ether at room temperature as reported by Fan et al.[22] The number in each marker of the plot corresponds to the molecule number it represents.

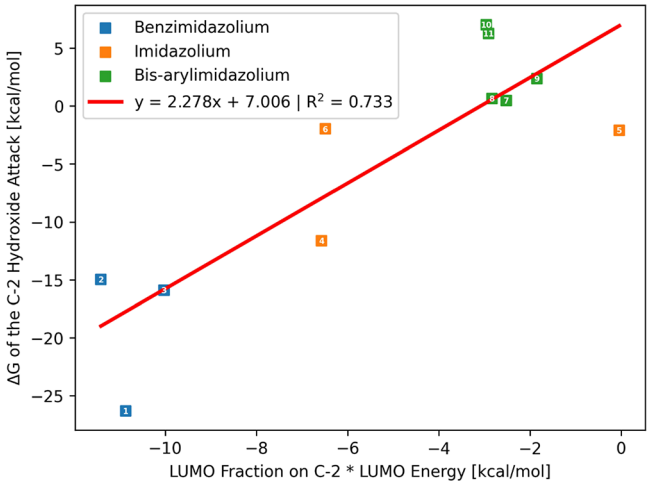

Figure 7. Scatter plot of the product of the LUMO energy and the LUMO fraction localized on C-2 versus the experimental half-life in an ultradry KOH solution of DMSO/crown ether at room temperature as reported by Fan et al.[22] The number in each marker of the plot corresponds to the molecule number it represents.

−14.96 kcal/mol for molecules 1 and 2, respectively) that their alkaline stability was too low to measure in the harsh stability test conditions referenced in Figure 3, the two compounds were also studied by Fan et al.[22] under milder conditions (3 M $NaOD/D_2O/CD_3OD$ at 80 °C) and a significantly higher stability for molecule 2 was observed (half-life of <0.1 and 436 h for molecules 1 and 2, respectively). When comparing the two compounds, differences in ΔG and alkaline stability can be explained based on increased steric demand of the mesityl group over the phenyl group. Especially, the area around the C-2 atom is occupied by the two ortho methyl groups of the mesityl substituent, thereby sterically shielding it from hydroxide attack. One noteworthy aspect is that the direct steric interference between the substituents and the attacking hydroxide is not the only relevant steric contribution that occurs. During the C-2 hydroxide attack, the C-2 atom transforms from a planar sp^2 hybridization into the tetragonal sp^3 hybridization, thereby pushing the C-2 substituent toward the imidazolium ring and creating steric strain in the product structure as can be seen in Figure 8.

Different degrees of steric strain are, however, not the only aspect contributing to differences in alkaline stability. The three methyl groups of the mesityl group exhibit a pronounced impact on the geometry of the cation, leading to the plane of the mesityl's phenyl ring being orthogonal to the plane of the imidazolium ring (dihedral angle of about 90°). The phenyl ring of molecule 1 on the other hand is tilted, leading to a dihedral angle between the phenyl and imidazolium plane of about 60°. This nonorthogonality of the C-2 substituent of

Table 2. Molecular Structures of Three Selected Compounds and Their LUMO Energy along with the Fraction of the LUMO Localized on C-2 As Determined by Frontier Molecular Population Analysis

IUPAC Name (Molecule Number)	Structure	LUMO Distribution	LUMO Fraction on C-2	LUMO Energy [kcal/mol]
1,3-dimethyl-2-phenyl-1*H*-benzo[*d*]imidazol-3-ium **(1)**	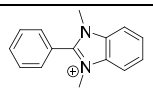	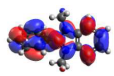	0.252	-43.168
1,3-dibutyl-2-mesityl-4,5-diphenyl-1H-imidazol-3-ium **(6)**	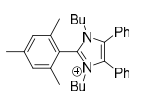	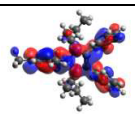	0.240	-27.009
2,2'-(2,3,5,6-tetramethyl-1,4-phenylene)bis(4,5-diphenyl-1,3-dipropyl-1*H*-imidazol-3-ium) **(10)**	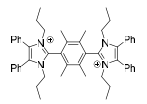	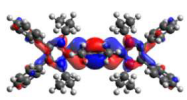	0.083	-35.616

https://doi.org/10.1021/acs.macromol.3c02294
Macromolecules 2024, 57, 1734−1743

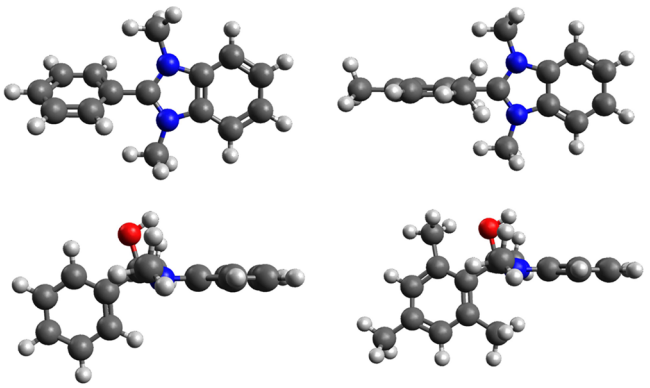

Figure 8. Optimized molecular structure of molecule **1** (left) and **2** (right) as the plain cation (top) and after a C-2 hydroxide attack (bottom).

molecule 1 is likely due to an interaction between the aromatic systems of the phenyl and the imidazolium ring, which in turn has an impact on the electronic structure of the cation. The significant difference in LUMO energy between molecules 1 and 2 (about −43 and −36 kcal/mol, respectively) is in part attributable to this difference in dihedral angle and also influences the C-2 hydroxide attack and, therefore, alkaline stability through this manner.

One aspect of the alkaline stability of imidazolium-based compounds highlighted by the identified energetic descriptor is the steric effect of the C-4 and C-5 substituents. While these two substituents generally do not directly sterically interfere with the attacking hydroxide, they can destabilize the C-2 hydroxide attack product. This effect can be seen by examining the structure of the C-2 hydroxide attack product of molecule 5 in Figure 9.

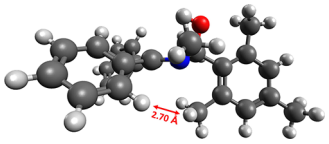

Figure 9. Illustration of the C-2 hydroxide attack product structure of molecule **5**. The figure highlights the proximity between the C-4/C-5 substituents with the C-2 substituent; the closest proximity is marked by a red double arrow and equals 2.70 Å.

As mentioned before, the C-2 hydroxide attack pushes the C-2 substituent toward the plane of the imidazolium through a change in the C-2 hybridization from sp^2 to sp^3. The steric strain from this structural change is enhanced by C-4 and C-5 substituents that protrude out of the imidazolium plane like the phenyl groups of molecule 5. This effect again emphasizes the complex structure−stability relationship of imidazolium-based compounds.

One significant electronic effect is noticeable among the bis-arylimidazolium moieties (molecules 10−14). They possess the highest stability of the studied compounds while having comparable steric demands at the C-2 site to molecule 6. This increased stability may be explained by their electronic structure, specifically their LUMO. The symmetric structure with two imidazolium groups leads to a distribution of the LUMO across the two imidazolium groups and a localization toward the central aryl group. Thereby, the LUMO is generally significantly less localized on the C-2 atom, leading to a decreased susceptibility toward hydroxide attack.

As this discussion for a limited number of molecules suggests, the relationship between the chemical structure and the alkaline stability is complex. Both electronic and steric effects are of relevance and must be considered for a sufficient understanding, especially as both effects may be intertwined. The benefit of an energetic descriptor such as ΔG of the C-2 hydroxide attack is that both steric and electronic effects and their interaction are intrinsically included. While a high-throughput scan of imidazolium-based compounds would be ideal to identify candidates with high alkaline stability, some qualitative trends toward alkaline stability could be identified from the molecules studied so far. One noteworthy aspect is that the steric demand of the C-4/C-5 substituents is also responsible for an increase in alkaline stability. Substitution at C-4/C-5 with sterically demanding groups that protrude out of the plane of the imidazolium ring may lead to an increase in stability, e.g., through 2,6-dimethylphenyl or mesityl. Additionally, the high alkaline stability of the bis-arylimidazolium compounds (molecules 10−14) was identified to likely stem from a diversion of the LUMO distribution away from the C-2 attack site. Additional stabilization might be possible through additional diversion, e.g., through a tris-arylimidazolium.

CONCLUSIONS

In this work, the electronic properties and energetics of the alkaline degradation pathways of (benz)imidazolium compounds were studied through quantum chemical computations. The calculated values were compared regarding experimental alkaline stability measurements by Fan et al. to identify suitable computational stability descriptors. This analysis yielded a computationally affordable strategy for assessing the alkaline stability of imidazolium compounds. It was found that ΔG of the C-2 hydroxide attack is a strong predictor for the alkaline stability in an ultradry alkaline environment. Additionally, in this work, the often-reported relationship between LUMO energy and alkaline stability could not be reproduced, implying that aspects such as degradation energetics or orbital distribution are more accurate stability predictors than the LUMO energy alone. A quantification method of the LUMO distribution was suggested by calculating the LUMO fraction localized on the C-2 atom. Utilizing these descriptors allows for a comprehensive investigation of the complex relationship between the chemical structure and alkaline stability of imidazolium-based compounds through qualitative structural analysis and high-throughput computations of potential molecules.

ASSOCIATED CONTENT

Supporting Information

The Supporting Information is available free of charge at https://pubs.acs.org/doi/10.1021/acs.macromol.3c02294.

Gibbs free energy profile of the dealkylation and the nucleophilic addition−elimination reaction of the studied compounds that are based on benzimidazolium; Gibbs free energy profile of the dealkylation and the nucleophilic addition−elimination reaction of the studied compounds that are based on imidazolium; Gibbs free energy profile of the dealkylation and the nucleophilic addition−elimination reaction of the studied compounds that are based on bis-arylimidazo-

https://doi.org/10.1021/acs.macromol.3c02294
Macromolecules 2024, 57, 1734−1743

lium; scatter plot of the ΔG of the nitrogen dealkylation and the experimental half-life (along with its natural logarithm) in an ultradry KOH solution of DMSO/crown ether at room temperature as reported by Fan et al.; scatter plot of the LUMO energy and the experimental half-life in an ultradry KOH solution of DMSO/crown ether at room temperature as reported by Fan et al.; selected electronic properties calculated for the studied compounds; selected electronic properties calculated for the studied compounds; and 11 studied molecular structures and their LUMO energy along with the fraction of the LUMO localized on C-2 as determined by a frontier molecular population analysis (PDF)

AUTHOR INFORMATION

Corresponding Author

Michael H. Eikerling − *Theory and Computation of Energy Materials (IEK-13), Institute of Energy and Climate Research, Forschungszentrum Jülich GmbH, 52425 Jülich, Germany; Chair of Theory and Computation of Energy Materials, Faculty of Georesources and Materials Engineering, RWTH Aachen University, Aachen 52062, Germany; Centre for Advanced Simulation and Analytics (CASA), Simulation and Data Science Lab for Energy Materials (SDL-EM), Forschungszentrum Jülich GmbH, Jülich 52425, Germany;* orcid.org/0000-0002-0764-8948; Email: m.eikerling@fz-juelich.de

Authors

Fabian P. Tipp − *Theory and Computation of Energy Materials (IEK-13), Institute of Energy and Climate Research, Forschungszentrum Jülich GmbH, 52425 Jülich, Germany; Centre for Advanced Simulation and Analytics (CASA), Simulation and Data Science Lab for Energy Materials (SDL-EM), Forschungszentrum Jülich GmbH, Jülich 52425, Germany;* orcid.org/0009-0009-6120-5660

Kate Fraser − *Department of Chemistry, Simon Fraser University, Burnaby, BC V5A 1S6, Canada*

Mohammad J. Eslamibidgoli − *Theory and Computation of Energy Materials (IEK-13), Institute of Energy and Climate Research, Forschungszentrum Jülich GmbH, 52425 Jülich, Germany; Centre for Advanced Simulation and Analytics (CASA), Simulation and Data Science Lab for Energy Materials (SDL-EM), Forschungszentrum Jülich GmbH, Jülich 52425, Germany;* orcid.org/0000-0002-5057-2993

Kourosh Malek − *Theory and Computation of Energy Materials (IEK-13), Institute of Energy and Climate Research, Forschungszentrum Jülich GmbH, 52425 Jülich, Germany; Centre for Advanced Simulation and Analytics (CASA), Simulation and Data Science Lab for Energy Materials (SDL-EM), Forschungszentrum Jülich GmbH, Jülich 52425, Germany;* orcid.org/0000-0002-3021-0813

Steven Holdcroft − *Department of Chemistry, Simon Fraser University, Burnaby, BC V5A 1S6, Canada;* orcid.org/0000-0002-1653-1047

Complete contact information is available at: https://pubs.acs.org/10.1021/acs.macromol.3c02294

Notes

The authors declare no competing financial interest.

ACKNOWLEDGMENTS

The authors acknowledge the financial support from the Federal Ministry of Education and Research (BMBF) under the German−Canadian Materials Acceleration Centre (GC-MAC) grant number 01DM21001A. They also gratefully acknowledge the Gauss Centre for Supercomputing e.V. (http://www.gauss-centre.eu) for funding this project by providing computing time through the John von Neumann Institute for Computing (NIC) on the GCS Supercomputer JUWELS[58] at Jülich Supercomputing Centre (JSC). The calculations were also enabled in part by computing resources provided by the Digital Research Alliance of Canada's Annual Resource Allocation Competition, Application ID 4544, "Advanced Polycation Design for Diverse Applications".

REFERENCES

(1) Hirscher, M.; Yartys, V. A.; Baricco, M.; von Colbe, J. B.; Blanchard, D.; Bowman, R. C., Jr.; Broom, D. P.; Buckley, C. E.; Chang, F.; Chen, P. Materials for hydrogen-based energy storage−past, recent progress and future outlook. *J. Alloys Compd.* **2020**, *827*, No. 153548.

(2) Zhang, F.; Zhao, P.; Niu, M.; Maddy, J. The survey of key technologies in hydrogen energy storage. *International journal of hydrogen energy* **2016**, *41* (33), 14535−14552.

(3) Kovač, A.; Paranos, M.; Marciuš, D. Hydrogen in energy transition: A review. *Int. J. Hydrogen Energy* **2021**, *46* (16), 10016−10035.

(4) Bernt, M.; Hartig-Weiß, A.; Tovini, M. F.; El-Sayed, H. A.; Schramm, C.; Schröter, J.; Gebauer, C.; Gasteiger, H. A. Current challenges in catalyst development for PEM water electrolyzers. *Chemie Ingenieur Technik* **2020**, *92* (1−2), 31−39.

(5) Kiemel, S.; Smolinka, T.; Lehner, F.; Full, J.; Sauer, A.; Miehe, R. Critical materials for water electrolysers at the example of the energy transition in Germany. *International Journal of Energy Research* **2021**, *45* (7), 9914−9935.

(6) Wang, J.; Gao, Y.; Kong, H.; Kim, J.; Choi, S.; Ciucci, F.; Hao, Y.; Yang, S.; Shao, Z.; Lim, J. Non-precious-metal catalysts for alkaline water electrolysis: operando characterizations, theoretical calculations, and recent advances. *Chem. Soc. Rev.* **2020**, *49* (24), 9154−9196.

(7) Merle, G.; Wessling, M.; Nijmeijer, K. Anion exchange membranes for alkaline fuel cells: A review. *J. Membr. Sci.* **2011**, *377* (1−2), 1−35.

(8) Du, N.; Roy, C.; Peach, R.; Turnbull, M.; Thiele, S.; Bock, C. Anion-exchange membrane water electrolyzers. *Chem. Rev.* **2022**, *122* (13), 11830−11895.

(9) Pan, Z.; An, L.; Zhao, T.; Tang, Z. Advances and challenges in alkaline anion exchange membrane fuel cells. *Prog. Energy Combust. Sci.* **2018**, *66*, 141−175.

(10) Das, G.; Choi, J.-H.; Nguyen, P. K. T.; Kim, D.-J.; Yoon, Y. S. Anion Exchange Membranes for Fuel Cell Application: A Review. *Polymers* **2022**, *14* (6), 1197.

(11) Yang, Z.; Guo, R.; Malpass-Evans, R.; Carta, M.; McKeown, N. B.; Guiver, M. D.; Wu, L.; Xu, T. Highly conductive anion-exchange membranes from microporous tröger's base polymers. *Angew. Chem.* **2016**, *128* (38), 11671−11674.

(12) Cheng, J.; He, G.; Zhang, F. A mini-review on anion exchange membranes for fuel cell applications: Stability issue and addressing strategies. *Int. J. Hydrogen Energy* **2015**, *40* (23), 7348−7360.

(13) Couture, G.; Alaaeddine, A.; Boschet, F.; Ameduri, B. Polymeric materials as anion-exchange membranes for alkaline fuel cells. *Prog. Polym. Sci.* **2011**, *36* (11), 1521−1557.

(14) Hagesteijn, K. F.; Jiang, S.; Ladewig, B. P. A review of the synthesis and characterization of anion exchange membranes. *J. Mater. Sci.* **2018**, *53* (16), 11131−11150.

(15) Arges, C. G.; Ramani, V. K.; Pintauro, P. N. The chalkboard: Anion exchange membrane fuel cells. *Electrochemical Society Interface* **2010**, *19* (2), 31.
(16) Mohanty, A. D.; Bae, C. Mechanistic analysis of ammonium cation stability for alkaline exchange membrane fuel cells. *Journal of Materials Chemistry A* **2014**, *2* (41), 17314−17320.
(17) Mohanty, A. D.; Tignor, S. E.; Sturgeon, M. R.; Long, H.; Pivovar, B. S.; Bae, C. Thermochemical stability study of alkyl-tethered quaternary ammonium cations for anion exchange membrane fuel cells. *J. Electrochem. Soc.* **2017**, *164* (13), F1279.
(18) Zhang, B.; Kaspar, R. B.; Gu, S.; Wang, J.; Zhuang, Z.; Yan, Y. A new alkali-stable phosphonium cation based on fundamental understanding of degradation mechanisms. *ChemSusChem* **2016**, *9* (17), 2374−2379.
(19) Gu, S.; Cai, R.; Luo, T.; Jensen, K.; Contreras, C.; Yan, Y. Quaternary phosphonium-based polymers as hydroxide exchange membranes. *ChemSusChem: Chemistry & Sustainability Energy & Materials* **2010**, *3* (5), 555−558.
(20) Marino, M.; Kreuer, K. Alkaline stability of quaternary ammonium cations for alkaline fuel cell membranes and ionic liquids. *ChemSusChem* **2015**, *8* (3), 513−523.
(21) Kim, D. S.; Fujimoto, C. H.; Hibbs, M. R.; Labouriau, A.; Choe, Y.-K.; Kim, Y. S. Resonance stabilized perfluorinated ionomers for alkaline membrane fuel cells. *Macromolecules* **2013**, *46* (19), 7826−7833.
(22) Fan, J.; Willdorf-Cohen, S.; Schibli, E. M.; Paula, Z.; Li, W.; Skalski, T. J.; Sergeenko, A. T.; Hohenadel, A.; Frisken, B. J.; Magliocca, E. Poly (bis-arylimidazoliums) possessing high hydroxide ion exchange capacity and high alkaline stability. *Nat. Commun.* **2019**, *10* (1), 2306.
(23) Fan, J.; Wright, A. G.; Britton, B.; Weissbach, T.; Skalski, T. J.; Ward, J.; Peckham, T. J.; Holdcroft, S. Cationic polyelectrolytes, stable in 10 M KOHaq at 100° C. *ACS Macro Lett.* **2017**, *6* (10), 1089−1093.
(24) Schibli, E. M.; Wright, A. G.; Holdcroft, S.; Frisken, B. J. Morphology of anion-conducting ionenes investigated by X-ray scattering and simulation. *J. Phys. Chem. B* **2018**, *122* (5), 1730−1737.
(25) Thomas, O. D.; Soo, K. J.; Peckham, T. J.; Kulkarni, M. P.; Holdcroft, S. Anion conducting poly (dialkyl benzimidazolium) salts. *Polym. Chem.* **2011**, *2* (8), 1641−1643.
(26) Thomas, O. D.; Soo, K. J.; Peckham, T. J.; Kulkarni, M. P.; Holdcroft, S. A stable hydroxide-conducting polymer. *J. Am. Chem. Soc.* **2012**, *134* (26), 10753−10756.
(27) Wright, A. G.; Weissbach, T.; Holdcroft, S. Poly (phenylene) and m-Terphenyl as Powerful Protecting Groups for the Preparation of Stable Organic Hydroxides. *Angew. Chem., Int. Ed.* **2016**, *55* (15), 4818−4821.
(28) Wei, Q.; Cao, X.; Veh, P.; Konovalova, A.; Mardle, P.; Overton, P.; Cassegrain, S.; Vierrath, S.; Breitwieser, M.; Holdcroft, S. On the stability of anion exchange membrane fuel cells incorporating polyimidazolium ionene (Aemion+®) membranes and ionomers. *Sustainable Energy & Fuels* **2022**, *6* (15), 3551−3564.
(29) Overton, P.; Li, W.; Cao, X.; Holdcroft, S. Tuning ion exchange capacity in hydroxide-stable poly (arylimidazolium) ionenes: increasing the ionic content decreases the dependence of conductivity and hydration on temperature and humidity. *Macromolecules* **2020**, *53* (23), 10548−10560.
(30) Wright, A. G.; Fan, J.; Britton, B.; Weissbach, T.; Lee, H.-F.; Kitching, E. A.; Peckham, T. J.; Holdcroft, S. Hexamethyl-p-terphenyl poly (benzimidazolium): a universal hydroxide-conducting polymer for energy conversion devices. *Energy Environ. Sci.* **2016**, *9* (6), 2130−2142.
(31) Hugar, K. M.; Kostalik, H. A., IV; Coates, G. W. Imidazolium cations with exceptional alkaline stability: a systematic study of structure−stability relationships. *J. Am. Chem. Soc.* **2015**, *137* (27), 8730−8737.
(32) Long, H.; Pivovar, B. Hydroxide degradation pathways for imidazolium cations: A DFT study. *J. Phys. Chem. C* **2014**, *118* (19), 9880−9888.
(33) Ye, Y.; Elabd, Y. A. Relative chemical stability of imidazolium-based alkaline anion exchange polymerized ionic liquids. *Macromolecules* **2011**, *44* (21), 8494−8503.
(34) Lin, B.; Dong, H.; Li, Y.; Si, Z.; Gu, F.; Yan, F. Alkaline stable C2-substituted imidazolium-based anion-exchange membranes. *Chem. Mater.* **2013**, *25* (9), 1858−1867.
(35) Gu, F.; Dong, H.; Li, Y.; Si, Z.; Yan, F. Highly stable N3-substituted imidazolium-based alkaline anion exchange membranes: experimental studies and theoretical calculations. *Macromolecules* **2014**, *47* (1), 208−216.
(36) Hollóczki, O.; Terleczky, P.; Szieberth, D.; Mourgas, G.; Gudat, D.; Nyulászi, L. Hydrolysis of Imidazole-2-ylidenes. *J. Am. Chem. Soc.* **2011**, *133* (4), 780−789.
(37) Yang, Y.; Wang, J.; Zheng, J.; Li, S.; Zhang, S. A stable anion exchange membrane based on imidazolium salt for alkaline fuel cell. *Journal of membrane science* **2014**, *467*, 48−55.
(38) Kreuer, K.-D.; Jannasch, P. A practical method for measuring the ion exchange capacity decrease of hydroxide exchange membranes during intrinsic degradation. *J. Power Sources* **2018**, *375*, 361−366.
(39) Wang, W.; Wang, S.; Xie, X.; Ramani, V. Density functional theory study of hydroxide-ion induced degradation of imidazolium cations. *Int. J. Hydrogen Energy* **2014**, *39* (26), 14355−14361.
(40) Dong, H.; Gu, F.; Li, M.; Lin, B.; Si, Z.; Hou, T.; Yan, F.; Lee, S. T.; Li, Y. Improving the alkaline stability of imidazolium cations by substitution. *ChemPhysChem* **2014**, *15* (14), 3006−3014.
(41) Lee, B.; Yun, D.; Lee, J.-S.; Park, C. H.; Kim, T.-H. Development of highly alkaline stable OH−-conductors based on imidazolium cations with various substituents for anion exchange membrane-based alkaline fuel cells. *J. Phys. Chem. C* **2019**, *123* (22), 13508−13518.
(42) Liu, Y.; Wang, J.; Yang, Y.; Brenner, T. M.; Seifert, S. E.; Yan, Y.; Liberatore, M. W.; Herring, A. M. Anion transport in a chemically stable, sterically bulky α-C modified imidazolium functionalized anion exchange membrane. *J. Phys. Chem. C* **2014**, *118* (28), 15136−15145.
(43) Wang, J.; Gu, S.; Kaspar, R. B.; Zhang, B.; Yan, Y. Stabilizing the imidazolium cation in hydroxide-exchange membranes for fuel cells. *ChemSusChem* **2013**, *6* (11), 2079−2082.
(44) Neese, F.; Wennmohs, F.; Becker, U.; Riplinger, C. The ORCA quantum chemistry program package. *J. Chem. Phys.* **2020**, *152* (22), 224108.
(45) Krishnan, R.; Binkley, J. S.; Seeger, R.; Pople, J. A. Self-consistent molecular orbital methods. XX. A basis set for correlated wave functions. *J. Chem. Phys.* **1980**, *72* (1), 650−654.
(46) Frisch, M. J.; Pople, J. A.; Binkley, J. S. Self-consistent molecular orbital methods 25. Supplementary functions for Gaussian basis sets. *J. Chem. Phys.* **1984**, *80* (7), 3265−3269.
(47) Becke, A. D. Density-functional exchange-energy approximation with correct asymptotic behavior. *Phys. Rev. A* **1988**, *38* (6), 3098.
(48) Lee, C.; Yang, W.; Parr, R. G. Development of the Colle-Salvetti correlation-energy formula into a functional of the electron density. *Phys. Rev. B* **1988**, *37* (2), 785.
(49) Barone, V.; Cossi, M. Quantum calculation of molecular energies and energy gradients in solution by a conductor solvent model. *J. Phys. Chem. A* **1998**, *102* (11), 1995−2001.
(50) RDKit: Open-source cheminformatics. https://www.rdkit.org, DOI: 10.5281/zenodo.7541264.
(51) Pracht, P.; Bohle, F.; Grimme, S. Automated exploration of the low-energy chemical space with fast quantum chemical methods. *Phys. Chem. Chem. Phys.* **2020**, *22* (14), 7169−7192.
(52) Grimme, S. Exploration of chemical compound, conformer, and reaction space with meta-dynamics simulations based on tight-binding quantum chemical calculations. *J. Chem. Theory Comput.* **2019**, *15* (5), 2847−2862.
(53) Ásgeirsson, V.; Birgisson, B. O.; Bjornsson, R.; Becker, U.; Neese, F.; Riplinger, C.; Jónsson, H. Nudged elastic band method for molecular reactions using energy-weighted springs combined with eigenvector following. *J. Chem. Theory Comput.* **2021**, *17* (8), 4929−4945.

https://doi.org/10.1021/acs.macromol.3c02294
Macromolecules 2024, 57, 1734−1743

(54) Guo, Y.; Riplinger, C.; Becker, U.; Liakos, D. G.; Minenkov, Y.; Cavallo, L.; Neese, F. Communication: An improved linear scaling perturbative triples correction for the domain based local pair-natural orbital based singles and doubles coupled cluster method [DLPNO-CCSD (T)]. *J. Chem. Phys.* **2018**, *148* (1), No. 011101.
(55) Evans, M.; Polanyi, M. Further considerations on the thermodynamics of chemical equilibria and reaction rates. *Trans. Faraday Soc.* **1936**, *32*, 1333−1360.
(56) Bell, R.; The, P. theory of reactions involving proton transfers. *Proc. R. Soc. London, Ser. A* **1936**, *154* (882), 414−429.
(57) Arduengo, A. J., III; Dias, H. R.; Harlow, R. L.; Kline, M. Electronic stabilization of nucleophilic carbenes. *J. Am. Chem. Soc.* **1992**, *114* (14), 5530−5534.
(58) Krause, D. JUWELS: Modular Tier-0/1 supercomputer at the Jülich supercomputing centre. *J. Large-Scale Res. Facil.* **2019**, *5*, A135.

https://doi.org/10.1021/acs.macromol.3c02294
Macromolecules 2024, 57, 1734−1743